

Effects of Illumination During Anodization of Porous Silicon

C. TSAI, K.-H. LI, and J. C. CAMPBELL

Microelectronics Research Center

Department of Electrical and Computer Engineering
The University of Texas at Austin, Austin, Texas 78712

B. K. HANCE, M. F. ARENDT, and J. M. WHITE
S.-L. YAU and A. J. BARD

Department of Chemistry and Biochemistry
The University of Texas at Austin, Austin TX 78712

The effects of illumination during anodic etching of porous Si have been studied. For a fixed current density and anodization time, it has been observed that below a critical irradiance level, increasing the radiant flux density during anodization results in higher photoluminescence and a blue shift of the photoluminescence spectra. For irradiance above the critical value, the photoluminescence intensity decreases. Transmission Fourier-transform infrared spectroscopy, x-ray photoelectron spectroscopy and atomic force microscopy have been employed to investigate the effects of illumination on the characteristics of porous Si.

Key words: Porous Si, photoluminescence, illumination effect

INTRODUCTION

The realization of practical, Si-based light-emitting devices would have a significant impact on numerous technologies including optoelectronic integrated circuits, optical memories and logic, and advanced display systems. Previously, however, Si has exhibited extremely weak emission owing to its indirect bandgap. Recent observations of efficient, room-temperature visible emission from porous Si¹⁻³ have stimulated research and extensive debate on the physical mechanisms responsible for this luminescence. To date, the explanations that have been proposed can be categorized as (1) two dimensional quantum confinement in the microstructure of highly porous Si,^{1,3-7} or (2) the formation of a wide-bandgap material such as a-SiH_x⁸ or siloxene⁹ during anodization. Recent work¹⁰⁻¹² has shown that the photoluminescence (PL) intensity of porous Si significantly decreases when the samples are annealed in vacuum at temperatures >350°C. Transmission Fourier-transform infrared (FTIR) spectroscopy has shown that this decrease in PL intensity coincides with the desorption of hydrogen from the SiH₂ species. Also, it has been observed that predominant SiH termination results in weak photoluminescence, whereas the PL intensity is recovered when the SiH₂ is restored.¹¹ The link between the PL intensity and the SiH₂ concentration is corroborated in this paper, through a study of the PL spectra of porous Si samples formed by irradiance at various optical power levels during anodization. Transmission FTIR and atomic force microscopy (AFM) were used to measure the concentration of the surface Si hydride species and to monitor the morphology of

these porous Si samples, respectively. In addition, x-ray photoelectron spectroscopy (XPS) has been utilized to provide information on Si-Si and Si-O binding energies (BE) and the relative atomic concentration of O, Si, F, and C. We conclude that the level of irradiance during anodization effects the average dimensions of the porous Si microstructures, the concentration of Si hydride and Si oxide, and the types of chemical bonds that predominate near the surface. These effects, in turn, influence the PL intensity and the position of the peak of the emission spectrum.

EXPERIMENTAL PROCEDURE AND RESULTS

A. Sample Preparation

The porous Si samples were prepared on (100) oriented, boron-doped Si substrates (resistivity ≈ 1 Ωcm) using a Teflon sample holder¹³ in contact with a copper anode. Through a one-inch-diameter circular opening in the fixture, the portion of the wafer to be anodized was exposed to an electrolyte, consisting of 2 parts deionized water, 1 part acetone, and 1 part 49% HF. During anodization the wafer was illuminated with a tungsten lamp that had its peak intensity at 620 nm. The irradiance was measured with a Si power meter. During the 15 min anodization process, the current was maintained at 10 mA/cm². The anodization procedure was repeated for radiant flux levels of 2, 3, 4, 6, 8, and 10 mW. Visually, it appeared that the luminescence of as-formed porous Si samples, as monitored with excitation from a 365 nm UV lamp, peaked at shorter wavelengths with increasing illumination power.

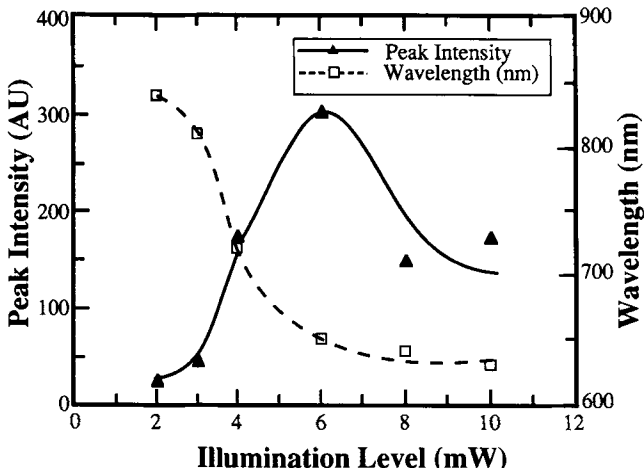


Fig. 1 — Intensity and wavelength of maximum luminescence vs illumination level during anodic etching.

B. Photoluminescence Measurements

After the samples were removed from the anodization chamber and dried in air, PL spectra were obtained with a 1-m scanning spectrometer and a photomultiplier with a GaAs photocathode. The optical pump for the luminescence was an Ar laser (power = 10 mW, $\lambda = 488$ nm). The laser beam was expanded to a diameter of 1 cm in order to avoid photoassisted degradation of the PL intensity.¹² Figure 1 shows that the PL peak intensity and the peak wavelength versus the illumination level during anodization. For illumination up to 6 mW, the PL intensity increases and the peak wavelength decreases. For irradiance >6 mW the PL intensity drops but the peak wavelength continues to decrease.

C. Transmission Fourier-transform Spectroscopy

With the sample under a nitrogen purge, the FTIR spectra were collected using a Mattson Cygnus 100 spectrometer equipped with a Triglycine Sulfate detector. Figure 2 shows the FTIR spectra for various irradiances during anodization. Peaks are seen at $2225\text{-}2050\text{ cm}^{-1}$, $1250\text{-}1000\text{ cm}^{-1}$, $950\text{-}875\text{ cm}^{-1}$, and 66 cm^{-1} . In addition, a shoulder at 1060 cm^{-1} appears for the 8 and 10 mW samples. The peaks from 2135 to 2089 cm^{-1} are generally attributed to the stretching modes of SiH and SiH₂. The peak at 1105 cm^{-1} corresponds to the bulk Si-O-Si asymmetric stretching mode and the 907 cm^{-1} peak is the scissors mode of SiH₂. The Si-O-Si peak is also present in nonporous Si. In addition, there is a Si-Si stretching mode at 617 cm^{-1} which is obscured by the deformation modes of the Si hydrides.¹⁴⁻¹⁵ The intensity of the SiH-SiH₂ stretch modes and the SiH₂ scissors mode increase with increasing illumination level up to 6 mW. However the intensity of these modes for 8 and 10 mW decreases to about the same strength as that for the 4 mW sample. The Si-Si stretching mode also increases up to 6 mW but above 6 mW, decreases to a strength lower than that at 2 mW. This indicates that pore surface area increases

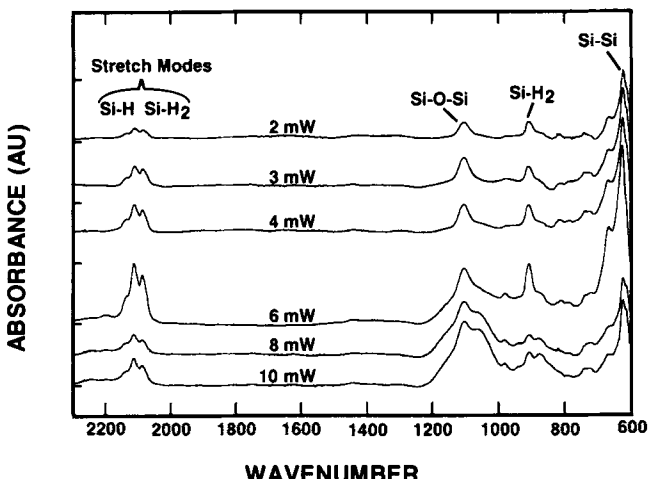


Fig. 2 — Transmission FTIR spectra for illumination levels of 2, 3, 4, 6, 8, and 10 mW.

with illumination from 2 to 6 mW but decreases for the high porosity 8 and 10 mW samples. On the other hand, the Si-O-Si peak continues to increase with illumination up to 10 mW, which indicates that more Si is oxidized for samples of higher optical powers.

D. Atomic Force Microscopy

The AFM used in this study was a commercial Nanoscope II (Digital Instrument Inc, Santa Barbara, CA). It utilized microfabricated V-shaped Si nitride cantilevers (100 μm long, wide legs) onto which sharp tips attached. Two scanners (15 μm and 1.0 μm) were able to achieve atomic resolution on atomically flat substrates such as newly cleaved pyrolytic graphite and mica. However, for rough samples such as the porous Si, the smaller scanner provided better resolution. In the present study, the larger scanner, which can resolve lateral surface feature areas as small as 0.05 nm^2 , was used to reveal the typical features of the porous Si samples and the higher resolution scanner was employed as a check. The vertical resolution depends on the local environment of the tip and the morphology of the porous Si samples. The scanner was calibrated against a Au ruling and the error was less than 10% under low thermal drift. All the AFM images reported here were obtained by the constant deflection mode, *i.e.* a feedback loop adjusted the piezo scanner so that a constant vertical force was maintained as the probe scanned across the surface. The AFM surface tracking ability was also profoundly affected by the shape of the probe and several cantilevers were used to assure optimum AFM resolution. Figure 3 (a), (b) and (c) shows the AFM images of the surface of porous Si for the 2, 6 and 10 mW samples, respectively. The lateral feature size at the surface of the samples monotonically decreases with increasing illumination level during anodization. We note that characteristic features <10 nm were not observed.

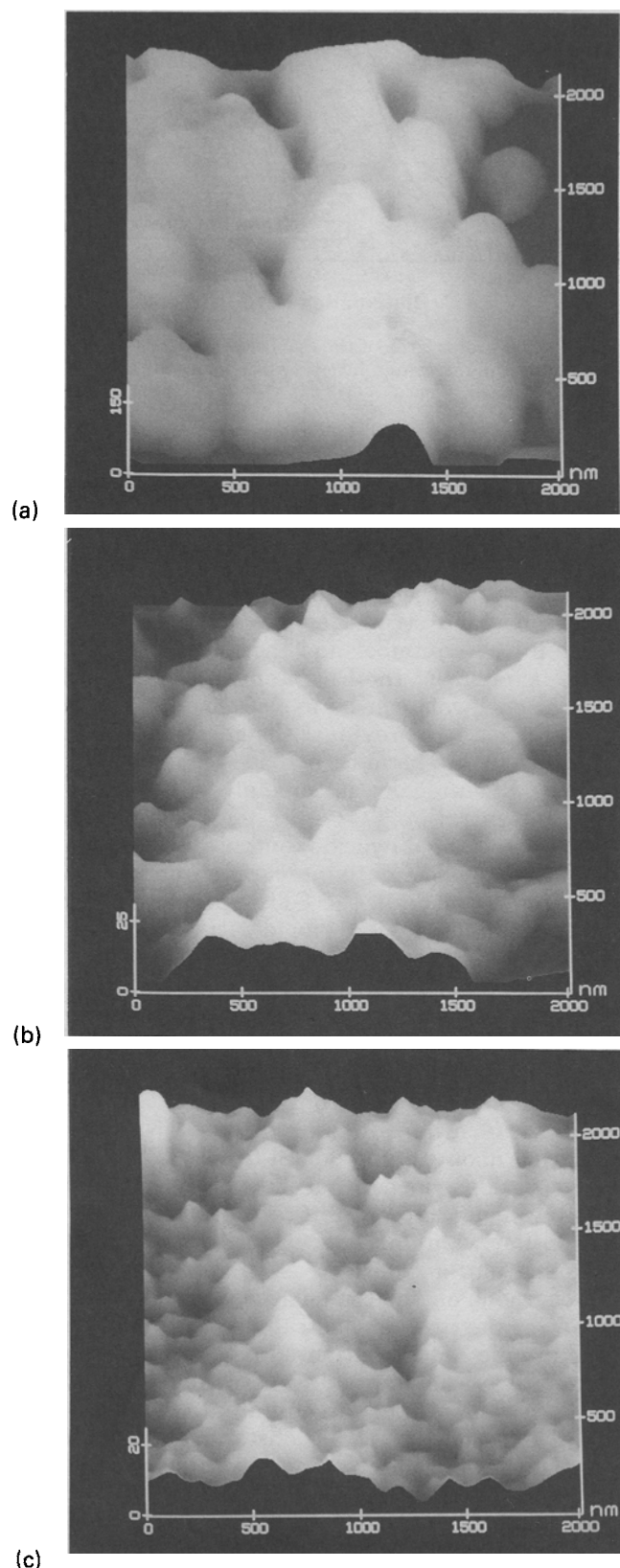


Fig. 3 — Images taken by atomic force microscopy for illumination levels of (a) 2 mW, (b) 6 mW, and (c) 10 mW.

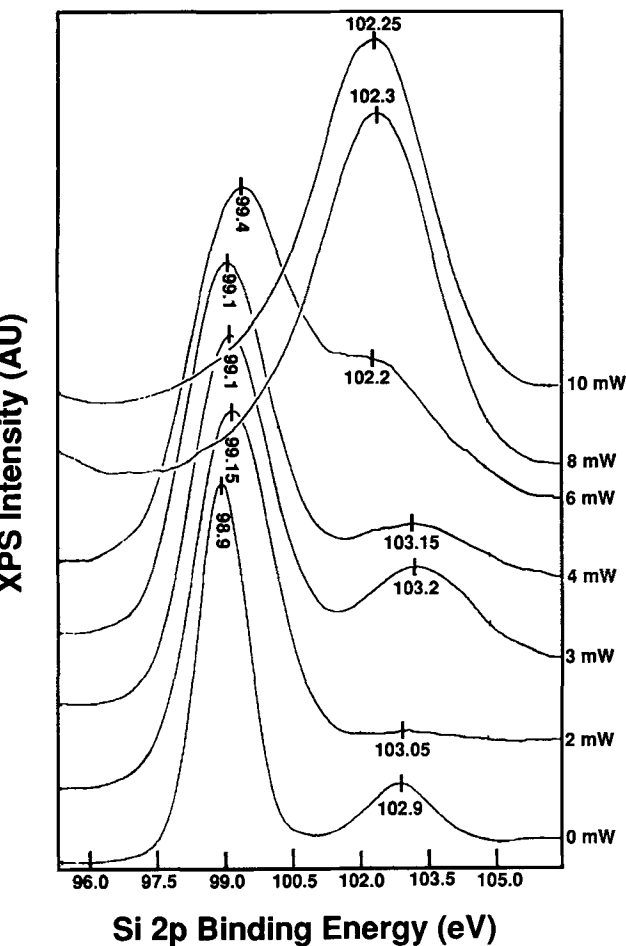


Fig. 4 — XPS spectra of Si 2p HV (Si-O) and LV (Si-Si) for porous Si.

E. X-ray Photoelectron Spectroscopy

XPS analysis was performed in a Vacuum Generator ESCALAB MARK I (Mg K α source, 330 W, 50 eV pass energy). Si 2p photoelectrons in SiO_2 with a mean free path of approximately 25 Å correspond to the maximum escape depth for the elements investigated in this Si/ SiO_2 system.²⁰ Correction for x-ray induced charging of each sample was accomplished by referencing the aliphatic C 1s binding energy to 284.6 eV.^{21–22} Binding energy was calculated at the centroid of the respective peak and then charge corrected. The relative elemental atomic concentrations with the XPS sampling volume were determined from their respective peak areas and V6 elemental sensitivity factors. The relative abundance of high valence silicon (HV), 102.2 ~ 103.2 eV, and low valence (LV) silicon, 98.9 ~ 99.4 eV, e.g., Si-O and Si-Si respectively, was measured from their respective Si (2p) Gaussian/Lorentzian curve-fitted peak areas. The Si 2p spectra in Fig. 4 illustrate the change in the oxidation state of the anodized porous Si as a function of illumination power. The peak centroids are marked and labeled with the charge corrected binding energy. Figure 5 shows the relative atomic concentrations of Si_{HV} , Si_{LV} , O, C, and F for the anodized porous Si surfaces as a function of illumination powers.

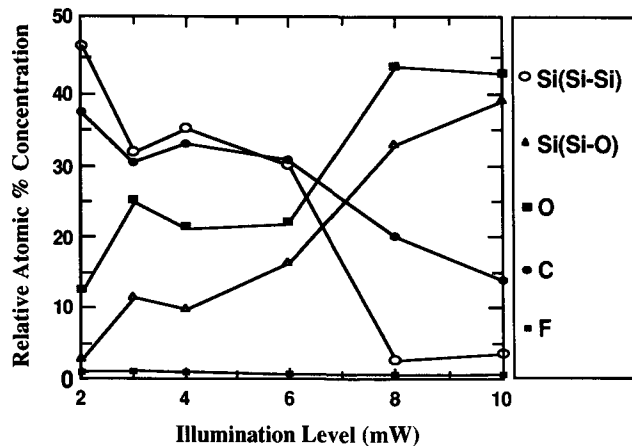


Fig. 5 — The relative atomic concentration of porous Si for different illumination levels during anodization.

DISCUSSION

It is clear from the AFM measurements that one effect of illumination is to reduce the lateral feature size at the surface relative to the samples anodized in the dark. Since AFM is a surface measurement technique it does not necessarily follow that the decreased feature size observed by AFM extends deep into the porous layer where optical absorption and recombination are strong. On the other hand, we observed that the decrease in lateral feature size coincides with an increase in porosity which would be consistent with a strong correlation between the AFM results and an "average" feature size. The increase in porosity and decrease in feature size are due to enhanced chemical dissolution and the increased photogenerated carrier density. It has been observed that the chemical dissolution of porous Si in HF solutions is greatly enhanced in the presence of light and that the PL peak wavelength can be shifted from 720 nm to 560 nm for a chemical dissolution time of only 6 min.¹⁶ It has been reported that if the walls between pores are depleted of holes (h^+) they will be protected against anodic dissolution.¹⁹ Therefore, we expect illumination during anodization to supply the photogenerated holes to the walls, which will result in a decrease in the feature size. On the other hand, if we had used degenerately doped degenerate *n*- and *p*-type samples, the reduction in the feature size due to illumination would not be expected.

Since the hydrogen surface concentration per unit area remains constant for the as-anodized samples, the intensity of the Si hydride stretching mode would be expected to represent the total surface area. In Fig. 2, we observe that the Si hydride stretching mode increases up to 6 mW but decreases for higher levels of illumination, which indicates that the total surface area increases up to 6 mW but decrease for 8 and 10 mW. In Fig. 2, it is also shown that the Si-Si stretching mode increases up to 6 mW but decreases for higher levels of illumination whereas the Si-O-Si peak continues to increase with illumination up to 10 mW. This means that some Si is consumed and oxidizes more at higher illumination

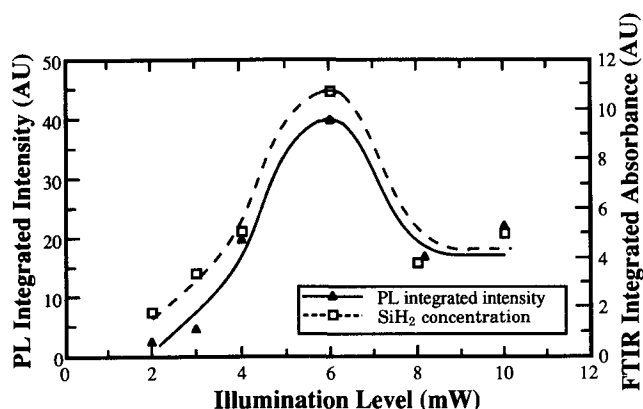


Fig. 6 — Integrated area of the SiH_2 scissors mode in the FTIR spectra and the integrated intensity of photoluminescence vs illumination level.

levels. We infer that as the dimensions of the microstructures become very small for 8 and 10 mW, the etching in the electrolyte and the oxidation of the Si, are sufficient to consume the smaller microstructures and lose the surface area contributed by these consumed structures, resulting in a net decrease in their number and the total surface area.

The behavior of the PL intensity for different illumination levels can be explained in terms of Si-H bonding. It has previously been reported that the porous Si layers have Si hydride-rich surfaces and that the PL intensity is correlated to the Si dihydride concentration.^{10–12,17–18} Figure 6 shows the PL intensity and the dihydride concentration, which has been determined from the integrated intensity of the SiH_2 scissors mode in the FTIR spectra, versus the illumination level during anodization. The increase in SiH_2 leads to an increase in the PL intensity. Above the critical illumination level the consumption of the smaller microstructures leads to a decrease in the Si dihydride species concentration and the PL intensity.

Although XPS probes only the first 25 Å of material at the surface it can still reveal valuable information about the porous Si layer. XPS measurements provide evidence that increasing irradiant flux density during anodization results in a decrease in the Si relative atomic concentration, an increase in the oxidation, and a decrease in the adsorption of hydrocarbons on the top surface of porous Si layer. These results are demonstrated in Fig. 5. The relative atomic concentration of oxygen in the porous surface layers increases by more than three folds, for a five-fold increase in illumination level, while the air exposure time was constant for all the samples. This is consistent with the increases in the Si-O-Si FTIR peak with increasing illumination and corroborates the picture of complete oxidation of the smallest Si microstructures.

The O 1s binding energies, Si 2p chemical shifts, and the energy differences between O 1s and Si 2p HV core-orbitals, listed in Tables I and II, reveal two different compositional regimes. Figures 4 and 5 graphically illustrate Regimes 1 and 2. For Re-

Table I. Si 2p HV, Si 2p LV, O 1s, and F 1s Binding Energies

| Illumination Level (mW) | LV Si 2p BE (eV) | HV Si 2p BE (eV) | O 1s BE (eV) | F 1s BE (eV) | Correction for Charging |
|-------------------------|------------------|------------------|--------------|--------------|-------------------------|
| | | | | | |
| 2 | 99.15 | 103.05 | 532.35 | 687.90 | 1.0 |
| 3 | 99.10 | 103.20 | 532.85 | 687.40 | 1.2 |
| 4 | 99.10 | 103.15 | 532.85 | 687.30 | 1.7 |
| 6 | 99.40 | 102.20 | 532.45 | 687.20 | 2.7 |
| 8 | 100.00 | 102.30 | 532.35 | 686.90 | 4.9 |
| 10 | 99.80 | 102.25 | 532.45 | 687.15 | 5.3 |
| Unanodized (100) c-Si | 98.90 | 102.90 | 532.40 | N/A | 0.5 |

gime 1, represented by the 2, 3, and 4 mW samples, the increase in surface oxide is accompanied by an increase in O 1s binding energies and Si 2p chemical shift. The surfaces of Regime 1 exhibit surface compositions similar to HF treated (100) single-crystal Si. However, the transition from Regime 1 to Regime 2, is distinct and characterized by approximately 0.7 eV increase in binding energy differences between O 1s and high valence Si 2p, approximately 1 eV drop in the Si 2p chemical shifts and a doubling of the oxide coverage of the surface of the Regime 2 samples.

Table I shows that the O 1s binding energies and the binding energy differences between O 1s and Si_{HV} 2p for the oxides of Regime 1 lie between 532.35–532.85 eV and 429.3–429.7 eV, respectively. Table II shows that their Si 2p chemical shifts lie between 4 and 4.3 eV. These values have been identified with SiO₂ films with thicknesses in the range from ~3 Å to ~40 Å.^{24–29} From Fig. 4 we see that for the samples represented by Regime 1 the low valence Si signal predominates, which is characteristic of a thin oxide on a crystalline substrate.

The low valence Si 2p binding energies (99.4–100 eV) for the samples of Regime 2 clearly show that Si-Si bonding no longer predominates the XPS sampling volume. The Si 2p chemical shifts (3.3–3.4 eV) of Regime 2, shown in Table II, are not consistent with the chemical shifts observed in stoichiometric

SiO₂ films. Grunder *et al.*,²¹ point out that similar chemical shifts are associated with oxides of intermediate compositions and the remaining bonds are not only Si-Si but could be units of the type Si-[O₃H] and Si-[O₂H₂]. From Table I an approximation of the silicon to oxygen stoichiometry (% O/% Si_{HV}) for Regime 2 shows oxide compositions of SiO_{1.4}, SiO_{1.3}, and SiO_{1.1} for samples 6, 8, and 10 mW, respectively. This shows that higher illumination levels causes more internal Si-O-Si bridges and oxygen backbonded Si-H groups, and that the SiO_{1.4} is characteristic of samples with the maximum PL intensity. The 6 mW sample has the chemical shift characteristics of Regime 2 but from Figs. 4 and 5 it is clear that the Si concentration still dominates the XPS sampling volume. XPS and FTIR show that the 6 mW sample corresponds to an ideal set of anodization and illumination conditions so that the degree of dissolution of the Si lattice maximizes SiH₂ species formation.

CONCLUSION

In conclusion, we have observed that illumination during anodic etching reduces the size of the microstructures in porous Si relative to samples prepared in the dark. This gives rise to a blue shift in the PL spectral peak. It is shown that for a given current density and etching time, the pore density (based on AFM) and surface area (based on FTIR) increases with increasing illumination up to a critical level. In this regime, the PL intensity and the Si dihydride concentration, as determined by FTIR measurements, also increase with illumination level. This correlation between PL intensity and the Si dihydride concentration is consistent with previous studies of the PL characteristics of porous Si. Illumination above the critical level removes the smaller structures through oxidation or complete chemical dissolution. In this regime, XPS measurements show increases in the Si-O-Si bridges and oxygen backbonded Si-H groups in the sampling volume on the top surface of porous Si. The observed increase in oxidation and the resulting decrease in surface area result in less SiH₂ and a concomitant decrease in the PL intensity.

ACKNOWLEDGMENT

We are grateful to Al. Tasch, D.-L. Kwong and B. G. Streetman for encouragement and helpful discussions and to C. M. Mathew for the help in the FTIR measurements. We thank MEMC Electronic Materials, Inc. for supplying the Si wafers used in this work. This work has been supported by grants from Office of Naval Research (ONR-N00014-92-J-1085), the Texas Advanced Research Program-178 and the NSF-supported Sci. and Techn. Ctr. at the University of Texas at Austin (CHE-8920120).

Table II. Si 2p Chemical Shift and Binding Energy Difference.

| Illumination Level (mW) | Si 2p Chemical Shift (eV) | Si 2p BE _{LV*} Difference (eV) | BE** (eV) |
|-------------------------|---------------------------|---|--------------------------|
| | | | O 1s-Si 2p _{HV} |
| 2 | 4.15 | 0.25 | 429.30 |
| 3 | 4.30 | 0.20 | 429.65 |
| 4 | 4.25 | 0.20 | 429.70 |
| 6 | 3.30 | 0.50 | 430.25 |
| 8 | 3.40 | 1.10 | 430.05 |
| 10 | 3.35 | 0.90 | 430.20 |
| Unanodized (100) c-Si | 4.00 | 0.00 | 429.50 |

*The binding energy difference between the respective sample's Si 2p low valence peak and the low valence Si 2p peak of (100) c-Si 98.9 eV.

**The binding energy difference between O 1s and the HV peak of Si.

REFERENCES

1. L. T. Canham, Appl. Phys. Lett. 57, 1046 (1990).

2. A. Halimaoui, C. Oules, G. Bomchil, A. Bsiesy, F. Gaspard, R. Herino, M. Ligeon and F. Muller, *Appl. Phys. Lett.* **59**, 304 (1991).
3. A. G. Cullis and L. T. Canham, *Nature. Lett.* **353**, 26 (1991).
4. T. D. Moustakas and J. S. Foresi, *MRS Meeting 1991 Fall, Symposium AA*.
5. K. P. Ghatak, *MRS Meeting 1991 Fall, Symposium AA*.
6. D. L. Naylor, S. Lee and J. Pincenti, *MRS Meeting 1991 Fall, Symposium AA*.
7. M. S. Hybertsen, *MRS Meeting 1991 Fall, Symposium AA*.
8. R. W. Fathauer, T. George, A. Ksendzov, T-L. Lir, W. T. Pike and R. P. Vasquez, *MRS Meeting 1991 Fall, Symposium AA*.
9. J. Weber, M. S. Brandt and H. D. Fuchs, M. Stutzmann, *MRS Meeting 1991 Fall, Symposium AA*.
10. C. Tsai, K.-H. Li, J. Sarathy, S. Shih, J. C. Campbell, B. Hance and J. M. White, *Appl. Phys. Lett.* **59**, 2814 (1991).
11. C. Tsai, K.-H. Li, D. Kinosky, R.-Z. Qian, T.-C. Hsu, J. Irby, S. Banerjee, A. Tasch, J. C. Campbell, B. K. Hance and J. M. White, to be published in *Appl. Phys. Lett.*
12. C. Tsai, K.-H. Li, J. C. Campbell, B. Hance and J. M. White, to be published in *J. Electrochem. Soc.*
13. P. Gupta, V. L. Colvin and S. M. George, *Phys. Rev. B* **37**, 8234 (1988).
14. M. H. Brodsky, M. Cardona and J. J. Cuomo, *Phys. Rev. B* **16**, 3356 (1977).
15. R. J. Collins and H. Y. Fan, *Phys. Rev.* **93**, 674 (1954).
16. A. Bsiesy, J. C. Vial, F. Gaspard, R. Herino, M. Ligeon, F. Muller, R. Romestain, A. Wasiela, A. Halimaoui and Bomchil, *Surf. Sci.* **254**, 195 (1991).
17. L. M. Peter, D. Blackwood and S. Pons, *Phys. Rev. Lett.* **62**, 308 (1989).
18. S. M. Prokes, O. J. Glembotck, V. M. Bermudez and R. Kaplans, *MRS Meeting 1991 Fall, Symposium AA*.
19. C. Tsai, K.-H. Li, J. Sarathy, S. Shih, K. H. Jung, D. L. Kwing and J. Campbell, *MRS Meeting 1991 Fall, Symposium AA*.
20. V. Lehmann and U. Gösele, *Appl. Phys. Lett.* **58**, 856 (1991).
21. R. Flitsch and R. Raider, *J. Vac. Sci. Technol.* **12**, 305 (1975).
22. M. Grundner and H. Jacob, *Appl. Phys. A* **39**, 73 (1986).
23. C. D. Wagner, W. M. Riggs, L. E. Davis, J. K. Moulder and G. E. Muilenberg, *Handbook of Photoelectron Spectroscopy*, Perkin-Elmer Corp, 17 (1979).
24. L. A. Zazzera and J. F. Moulder, unpublished.
25. F. J. Grunthaner, P. J. Grunthaner, R. P. Vasquez, B. F. Lewis, J. Maserjian and A. Madhukar, *J. Vac. Sci. Technol.* **16**, 1443 (1979).
26. G. Hollinger, Y. Jugnet, P. Pertosa and T.-M. Duc, *Chem. Phys. Lett.* **36**, 443 (1975).
27. G. Hollinger, J. F. Morar, G. Hughes and J. L. Jordan, *Surf. Sci.* **168**, 609 (1986).
28. P. J. Grunthaner, M. H. Hecht, F. J. Grunthaner and N. M. Johnson, *J. Appl. Phys.* **61**, 629 (1987).
29. G. Hollinger and F. J. Hempsel, *Appl. Phys. Lett.* **44**, 613 (1984).